

## IMAGE PROCESSING AND COMPOSITION STUDIES OF NANOPARTICLES FROM OLEYLAMINE REDUCTION OF IRON AND PLATINUM ACETYLACETONATES

Y. SIRISATHITKUL<sup>a,b,1</sup>, P. SARMPHIM<sup>c</sup>, C. SIRISATHITKUL<sup>b,d</sup>

<sup>a</sup>*School of Informatics, Walailak University, Nakhon Si Thammarat, Thailand*

<sup>b</sup>*Functional Materials and Nanotechnology Center of Excellence, Walailak University, Nakhon Si Thammarat, Thailand*

<sup>c</sup>*Department of General Education, Faculty of Liberal Arts, Rajamangala University of Technology Srivijaya, Songkhla, Thailand*

<sup>d</sup>*Department of Physics, School of Science, Walailak University, Nakhon Si Thammarat, Thailand*

Iron-platinum nanoparticles are under investigation for their superparamagnetic properties in biomedical applications. In this work, nanoparticles around 5 nm in diameter were obtained from the co-reduction of iron(III) acetylacetonate ( $\text{Fe}(\text{acac})_3$ ) and platinum(II) acetylacetonate ( $\text{Pt}(\text{acac})_2$ ) without using traditional solvents and reducing agents. In addition to its role as a surfactant, oleylamine was used to dissolve  $\text{Fe}(\text{acac})_3$  and  $\text{Pt}(\text{acac})_2$  in the first synthesis step. In the final step, oleic acid was added to enhance the dispersion in hexane. By drop-casting the nanosuspension on substrates, composition and size distributions can be respectively studied by transmission electron microscopy (TEM) image processing and energy dispersive spectroscopy (EDS). Nanoparticles mostly aggregated into short chains and formed multilayers. The observed areas are classified into three categories according to the variation in composition measured by EDS. A balanced composition between Fe and Pt was only obtained in some areas. Pt was predominantly detected in several areas whereas iron oxide were also found in other areas with high amounts of O and Fe. As described by the heterocoagulation model, the difference in Fe and Pt nucleation rates led to Pt-rich cores surrounded by iron oxides. Besides FePt,  $\text{FePt}_3$  phase was subsequently formed as confirmed by selected-area electron diffraction (SAED).

(Received May 30, 2019; Accepted July 14, 2019)

**Keywords:** Iron-platinum nanoparticles, Oleylamine, energy dispersive spectroscopy, Transmission electron microscopy, Image processing

### 1. Introduction

Iron Platinum (FePt) nanoparticle with the face-centered cubic (fcc) structure exhibits superparamagnetic properties useful in biomedical applications [1,2]. Its advantages over the commonly used iron oxides and other magnetic nanoparticles are its high magnetic anisotropy and multi-functionality [3]. Furthermore, thermal diffusion of Fe atoms upon heat treatment results in the structural change into face-centered tetragonal (fct) as well as magnetic transition to ferromagnetism which has potential in ultrahigh density recording [4]. The traditional route to synthesize these FePt nanoparticles is by the thermal decomposition of iron pentacarbonyl ( $\text{Fe}(\text{CO})_5$ ) and the reduction of platinum(II) acetylacetonate ( $\text{Pt}(\text{acac})_2$ ) by reducing agents such as 1,2 hexadecanediol and  $\text{KBH}_4$  in ether solvents [5]. Oleic acid and oleylamine are also added as surfactants to prevent these nanoparticles from aggregation. Nanoparticles are stabilized by these surfactants without the sedimentation in carrier liquids. The optimum amount of surfactants has been investigated since either excessive or insufficient surfactants strongly affect the particle size obtained from the syntheses [2,5,6].

---

<sup>1</sup>Corresponding author: kinsywu@gmail.com

Since  $\text{Fe}(\text{CO})_5$  is highly toxic and volatile, the modified polyol process is developed using iron(III) acetylacetonate ( $\text{Fe}(\text{acac})_3$ ) as a replacement [7-9].  $\text{Fe}(\text{acac})_3$  and  $\text{Pt}(\text{acac})_2$  respectively decompose around 185 and 135 °C. The process is a simple, effective and environmental friendly. As suggested by Nandwana et al. [7], this reaction at moderate temperatures does not require a reducing agent. Nakaya and co-workers were the first group to use excess surfactants in the FePt nanoparticle synthesis without any conventional ether solvent [8]. Later, Yu et al. [10] demonstrated that CoPt, NiPt, CuPt, ZnPt nanoparticles could also be synthesized by oleylamine reduction of metal salts. More recently, the oleylamine reduction was adopted to synthesize Pt nanoparticles [11]. These Pt and Pt-based nanoalloys have attracted attentions for their catalytic properties [12].

In this work, FePt based nanoparticles is synthesized via the co-reduction of  $\text{Fe}(\text{acac})_3$  and  $\text{Pt}(\text{acac})_2$  by oleylamine instead of traditional ether solvents and reducing agents. An image processing of nanoparticles was performed to compare with experimental works in the literature and composition were analyzed according to the proposed heterocoagulation model [9].

## 2. Experimental

$\text{Fe}(\text{acac})_3$  (99.9%),  $\text{Pt}(\text{acac})_2$  (97%), oleylamine (70%), oleic acid (90%) of the analytical grade from Sigma-Aldrich Company were used as received. The synthesis in a standard Schlenk line without traditional solvent and reducing agent was adapted from that by Yu et al. [10]. Only 20 mL oleylamine was added to a 100 mL Schlenk flask containing 0.5 mmol  $\text{Fe}(\text{acac})_3$  and 0.5 mmol  $\text{Pt}(\text{acac})_2$ . Under constant stirring and  $\text{N}_2$  flow, the solution was heated to 300 °C for 1 h. The product from the reflux was then cooled to room temperature under  $\text{N}_2$  atmosphere. The particles were precipitated in ethanol and then centrifuged for 15 min. The obtained precipitates were re-dispersed in hexane and the purifying process was repeated twice. In the final dispersion in hexane, the oleic acid was added as an additional surfactant to stabilize the nanosuspension.

Nanoparticles were characterized by drop-casting the nanosuspension on carbon-coated copper grid substrate. Then, the morphology was visualized by a transmission electron microscopy (TEM; JEOL JEM-2010) and the phases were characterized by selected-area electron diffraction (SAED) in TEM. The distribution in intensity in different areas in TEM images was analyzed to distinguish monolayer from multilayer. To obtain a size distribution from a much larger sampling size than the common one-by-one inspections, the image processing in Matlab was performed. The image was partitioned into four portions due to uneven gray levels between objects and the background. A binary image was individually created by the Otsu's thresholding method each portion from its possible threshold values before combining with one another. Nanoparticles were detected by identifying their boundaries using the Canny edge detection algorithm. The closing, filling and noise removal steps were then successively implemented [13]. Finally, the number of particles and their average diameter were computed. The elemental composition in six locations was determined by an energy dispersive spectroscopy (EDS) probe attached to a field-emission scanning electron microscopy (FESEM; FEI Quanta 450 FEG).

## 3. Results and discussion

The synthesized nanoparticles are spheroidal and tend to assemble into short chains of 3-5 nanoparticles as shown by TEM images. According to the lowly magnified images in Figure 1, their spatial distribution in the approximately  $1.5 \mu\text{m}^2$  area are uneven with formation of both nanoparticle monolayer and multilayer. The monolayer with short range orders is characterized by areas with high intensity in the TEM image as exemplified by the inset (b) of Figure 1. By contrast, the intensity curve in the inset (c) is shifted to the darker scale corresponding to nanoparticle stacking into multilayers and the lowest intensity shown in the inset (a) indicate the severe aggregation.

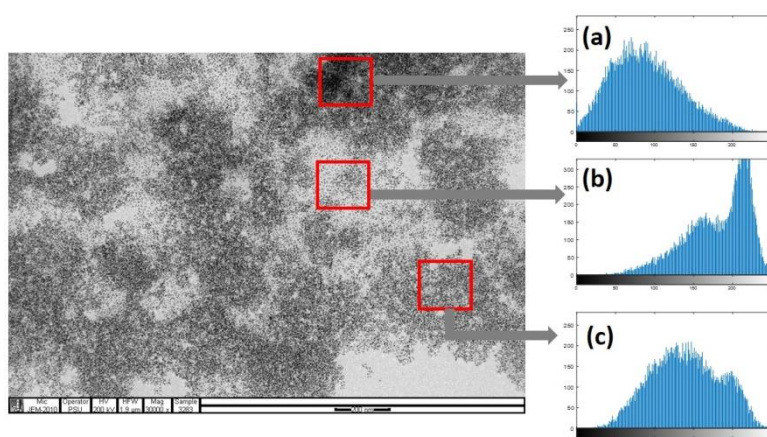


Fig. 1. Lower magnified TEM image of synthesized nanoparticles with the intensity analysis in the insets (a)-(c) from three areas.

With a higher magnification in Fig. 2, nanoparticles of 1076 in total are detected by the TEM image processing. Although a large number of particles in aggregation are missing from the detection as illustrated by Fig. 2(b), nanoparticles exceeding 1000 are statistically sufficient to represent products from the synthesis. The average diameter of  $5.6 \pm 3.5$  nm is slightly larger than those synthesized using the same precursors in benzyl ether [6] and dioctyl ether [14]. The distribution shown by the histogram and the standard deviation suggested that the nanoparticle size from this oleylamine reduction are comparable to those in the literature and sufficiently uniform for some biomedical applications.

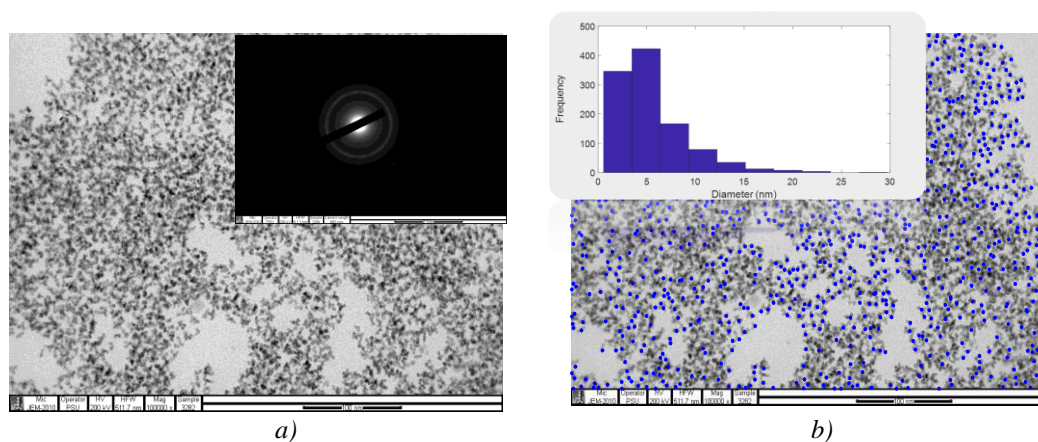


Fig. 2. Higher magnified TEM image of nanoparticles (a) before and (b) after image processing. The inset (a) shows a SAED rings and the inset (b) is a histogram of nanoparticle size distribution.

The SAED rings in inset of Fig. 2(a) correspond to the diffraction of (111), (200), (220), (311) planes of  $\text{FePt}_3$  [14]. Since the integrated-intensity diffraction pattern is influenced by the particle size, the obtained high intensity ring is in good agreement with the larger particle size analyzed by the image processing. Other set of low intensity SAED patterns are not clear enough for identifying other phases.

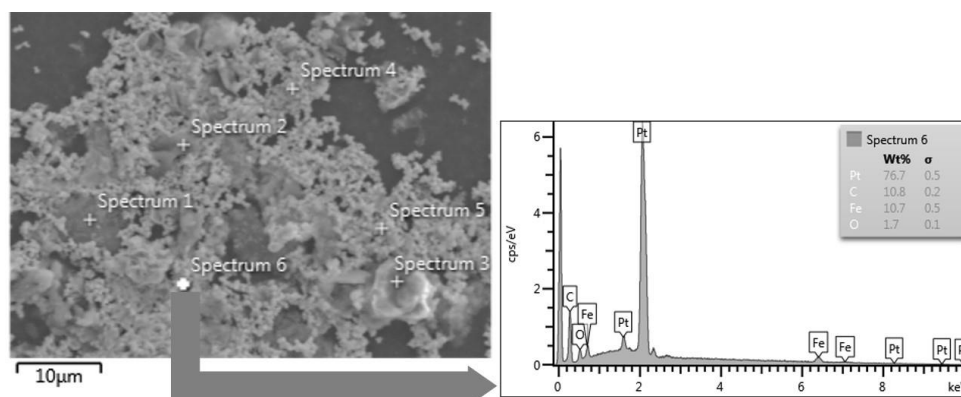


Fig. 3. FESEM image indicating six locations of EDS measurements. One EDS spectrum with Pt-rich nanoparticles is shown as an example.

Elemental compositions in Table 1 show a large variation with EDS-probed locations illustrated in Fig. 3. Spectra 4-6 indicate Pt-rich particles whereas Spectra 1-3 exhibit much larger amounts of C and O. Although the starting Fe:Pt ratio is not carried over to the final product, the amounts of Fe and Pt are comparable in Spectra 2 and 3. The presence of iron oxide is confirmed by the area exemplified by Spectrum 1 with around 24% of Fe and O. On the other hand, over 70% Pt is detected in Spectrum 4-6 and with a lower Fe:Pt ratio than 1:3 expected from  $\text{FePt}_3$ . The discrepancy between the EDS and SAED suggest that, in addition to  $\text{FePt}_3$  particles, Pt also exists in the zero valence state. Fe could be increased by the combination of an extra amount of  $\text{Fe}(\text{acac})_3$  and reducing agents as 1,2-hexadecanediol and  $\text{KBH}_4$ . However, such a combination may lead to a larger morphological variation in the final product and excess  $\text{Fe}_3\text{O}_4$  [6].

Table 1. Elemental compositions of nanoparticles measured from six locations by EDS.

Element	Spectrum 1	Spectrum 2	Spectrum 3	Spectrum 4	Spectrum 5	Spectrum 6
C	42.60	59.76	61.26	17.64	10.89	10.83
O	23.24	12.86	9.30	2.52	1.39	1.70
Fe	24.56	10.91	15.72	9.63	11.33	10.75
Pt	9.60	16.47	13.72	70.20	76.40	76.72

Whereas the  $\text{FePt}$  formation by thermal decomposition of  $\text{Fe}(\text{CO})_5$  is described by the binary nucleation model [15], the co-reduction is explained by the heterocoagulation model [9]. Pt-rich nuclei are initially formed and their surfaces are adsorbed by  $\text{Fe}_3\text{O}_4$  clusters and CO. High amounts of C and O in Spectra 1-3 are consistent with this model in which  $\text{Fe}(\text{acac})_3$  is harder to reduce and tends to form iron oxides. In the subsequent stage of  $\text{FePt}$  formation at high temperature,  $\text{Fe}_3\text{O}_4$  nanoparticles are reduced in the CO-spill over process and resulting Fe atoms then diffuse into Pt-rich nuclei. Harpeness and Gedanken suggested that the carbon atoms coated on the  $\text{FePt}$  nanoparticle surface facilitate the reduction into the metallic Fe [16]. It follows that there are large variations in composition and phase during the process. In the mixed phases, Pt-rich nuclei may also lead to  $\text{FePt}_3$  [14].

#### 4. Conclusions

$\text{Fe}(\text{acac})_3$  was used as a green alternative to highly toxic  $\text{Fe}(\text{CO})_5$  in the co-reduction with  $\text{Pt}(\text{acac})_2$ . With a single step heating to 300 °C, the synthesis was carried out using oleylamine instead of an ether solvent and oleic acid was only added in the final stage. Surface-modified nanoparticles were obtained with an average diameter of 5.6 nm comparable to those in the

literature but they tend to aggregate into short chains. Moreover, the nanoparticle stacking into multilayer occurs in some areas of high intensity in the TEM image. The elemental composition measured by EDS at six locations exhibited variations from Pt-rich nanoparticles, iron oxides as well as nanoparticles with a balanced composition between Fe and Pt.

### Acknowledgements

This project was partially supported by the New Strategic Research (P2P) project, Walailak University, Thailand. The authors would like to thank P. Harding and K. Chokprasombat for their suggestions. The technical assistance in TEM imaging by P. Pinsrithong of Scientific Equipment Center, Prince of Songkla University is acknowledged.

### References

- [1] P. Srinoi, Y.-T. Chen, V. Vittur, M. D. Marquez, T. R. Lee, *Applied Sciences* **8**(7), 1106 (2018).
- [2] Y. Shi, M. Lin, X. Jiang, S. Liang, *Journal of Nanomaterials* **2015**, 467873 (2015)
- [3] M. Gogoi, K. S. Varadarajan, A. B. Patel, P. Deb, *Acta Metallurgica Sinica English Letters* **29**(12), 1098 (2016).
- [4] S. A. Sebt, H. Zeynali, H. Arabia, H. Akbari, M. R. H. Zadeh, *Digest Journal of Nanomaterials and Biostructures* **7**(2), 745 (2012).
- [5] S. Sun, *Advanced Materials* **18**(4), 393 (2006).
- [6] K. Chokprasombat, P. Harding, C. Sirisathitkul, P. Muthitamongkol, S. Pinitsoontorn, *Indian Journal of Engineering and Materials Science* **19**(5), 338–342 (2012).
- [7] V. Nandwana, K. E. Elkins, J. P. Liu, *Nanotechnology*, **16**(12), 2823 (2005).
- [8] M. Nakaya, M. Kanehara, T. Teranishi, *Langmuir*, **22**(8), 3485 (2006).
- [9] W. Beck Jr, C. G. S. Souza, T. L. Silva, M. Jafellicci Jr, L. C. Varanda, *Journal of Physical Chemistry C* **115**(21), 10475 (2011).
- [10] Y. S. Yu, W. W. Yang, X. L. Sun, W. L. Zhu, X. Z. Li, D. J. Sellmyer, S. H. Sun, *Nano Letters* **14**(5), 2778 (2014).
- [11] Z. Zhao, A. Fisher, Y. Shen, D. Cheng, *Journal of Cluster Science* **27**(3), 817–843 (2016).
- [12] M. Y. Rekha, R. Akash, C. Srivastava, *National Academy of Science Letters* **41**(3), 169 (2018).
- [13] U. Phromsuwan, C. Sirisathitkul, Y. Sirisathitkul, B. Uyyanonvara, P. Muneesawang, *Journal of Magnetism* **18**(3), 311 (2013).
- [14] P. Sarmphim, S. Soontaranon, C. Sirisathitkul, P. Harding, S. Kijamnajsuk, B. Chayasombat, S. Pinitsoontorn, J. Chingunpitak, *Bulletin of the Polish Academy of Sciences Technical Sciences* **65**(1), 79 (2017).
- [15] S. Sun, E. E. Fullerton, D. Weller, C. B. Murray, *IEEE Transactions of Magnetism* **37**(4), 1239 (2001).
- [16] R. Harpeness, A. Gedanken, *Journal of Materials Chemistry* **15**(6), 698 (2005).